Faghirabadi *et al. Virology Journal* (2024) 21:235
https://doi.org/10.1186/s12985-024-02519-3

Virology Journal

RESEARCH Open Access

Intracellular delivery of antiviral shRNA using penetratin-based complexes effectively inhibits respiratory syncytial virus replication and host cell apoptosis

Faezeh Faghirabadi[1†], Haniyeh Abuei[1†], Mohammad Hossein Malekzadeh[1], Anahita Mojiri[2] and Ali Farhadi[1,3*]

Abstract

Background Cell-penetrating peptides (CPPs) are effective for delivering therapeutic molecules with minimal toxicity. This study focuses on the use of penetratin, a well-characterized CPP, to deliver a DNA vector encoding short hairpin RNA (shRNA) targeting the respiratory syncytial virus (RSV) F gene into infected cells. RSV is known to cause severe lower respiratory infections in infants and poses significant risks to immunocompromised individuals and the elderly. We evaluated the antiviral efficacy of the penetratin-shRNA complex by comparing its ability to inhibit RSV replication and induce apoptosis with ribavirin treatment.

Methods Penetratin-shRNA complexes were prepared at different ratios and analyzed using gel retardation assays, dynamic light scattering, and zeta potential measurements. The complexes were tested in HEp-2 and A549 cells for transfection efficiency, cytotoxicity, viral load, and apoptosis using plaque assays, real-time reverse transcription-polymerase chain reaction (RT-PCR), DNA fragmentation, propidium iodide staining, and caspase 3/7 activation assays.

Results The gel shift assay determined that a 20:1 CPP-to-shRNA ratio was optimal for effective complexation, resulting in particles with a size of 164 nm and a zeta potential of 8.7 mV. Transfection efficiency in HEp-2 cells was highest at this ratio, reaching up to 93%. The penetratin-shRNA complex effectively silenced the RSV F gene, reduced viral titers, and decreased DNA fragmentation and apoptosis in infected cells.

Conclusion Penetratin effectively delivers shRNA targeting the RSV F gene, significantly reducing viral load and preventing apoptosis without toxicity. This approach surpasses Lipofectamine and shows potential for future therapeutic interventions, especially when combined with ribavirin, against RSV infection.

†Faezeh Faghirabadi and Haniyeh Abuei contributed equally to this work.

*Correspondence:
Ali Farhadi
Farhadi_a@sums.ac.ir

Full list of author information is available at the end of the article

Graphical Abstract

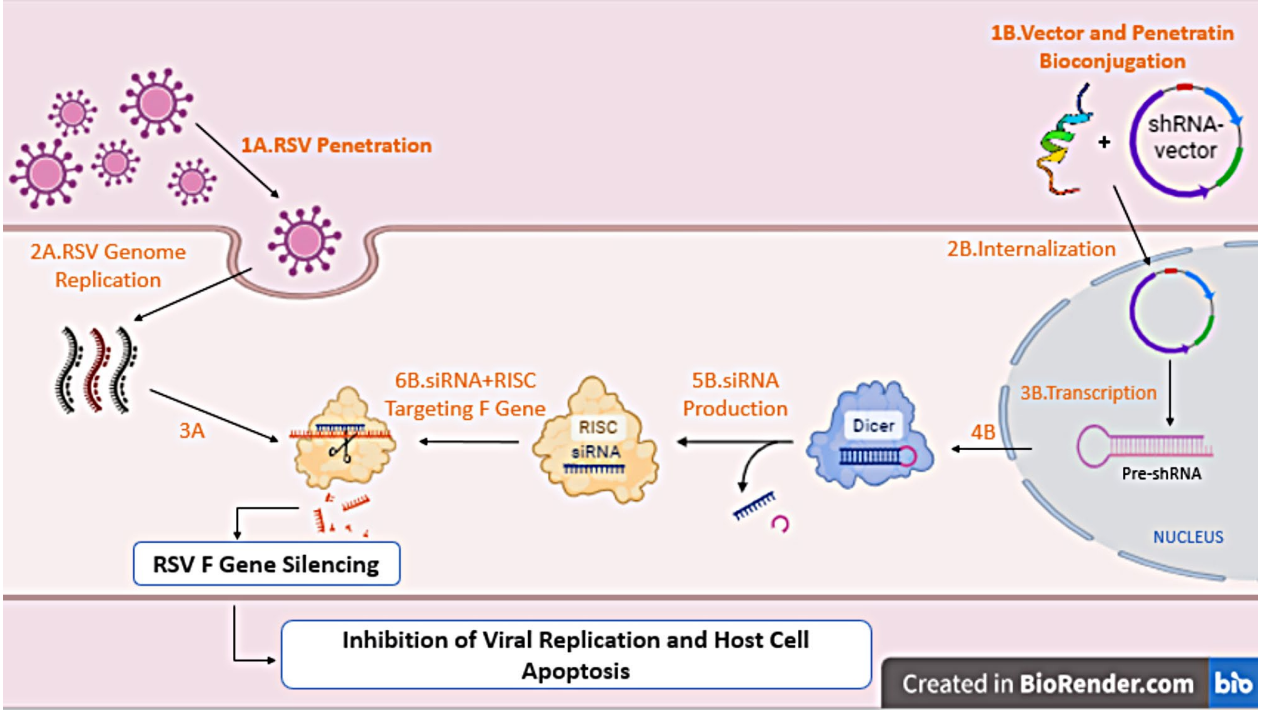

Keywords Human respiratory syncytial virus, shRNA, Penetratin, Cell-penetrating peptides, Ribavirin, Fusion gene, Apoptosis

Background

In recent decades, cell-penetrating peptides (CPPs) have been widely used as carriers for delivering oligonucleic acids, plasmids, and other drugs into cells [1]. These molecules exhibit a remarkable ability to penetrate the cell membrane at low concentrations, both in vitro and in vivo, without causing damage [2]. Recent studies have also demonstrated their minimal toxicity in cells [3]. Typically consisting of 5 to 30 amino acids, CPPs can be conjugated to biological macromolecules, such as oligonucleic acids and plasmids, both covalently and non-covalently, facilitating the entry of these biomolecules into cells [4, 5]. When forming a non-covalent conjugation between CPPs and cargo via electrostatic bonds, the nature of both molecules is preserved, suggesting the superiority of non-covalent bonds over covalent ones [6, 7].

Penetratin (PEN) is one of the first CPPs discovered, composed of 16 amino acids and bearing a positive charge [8]. Derived from the homeodomain of antennapedia, a Drosophila transcription factor, penetratin serves as an effective vector for the intracellular delivery of peptides or oligonucleotides [9]. Its characteristic binding to the DNA of homeodomains inspires the use of penetratin as a vector for the delivery of pDNA and oligonucleotides into cells [10]. RNA interference (RNAi) is a gene silencing mechanism in which the RNA-induced silencing complex (RISC) carries a small antisense RNA oligonucleotide [11]. This RNA strand binds to its target RNA through Watson–Crick base pairs. Upon complete base pairing, the RNAi mechanism initiates cleavage of the target RNA, leading to gene silencing [12]. The induction of RNAi can silence genes in mammalian cells for therapeutic purposes, such as combating viral infections. Small interfering RNA (siRNA) and short hairpin RNA (shRNA) serve as artificial inducers of the RNAi pathway [13]. siRNA enters the cell as two oligonucleotide strands, with the antisense strand being activated by RISC and binding to its complementary target RNA. Argonaute 2 (Ago2), present in RISC, catalyzes the cleavage of the target RNA [14]. ShRNA can be introduced into cells via plasmids or viral vectors. After delivery into the cell, hairpin precursors of these DNA vectors are expressed in the nucleus. These precursors undergo processing in the nucleus before entering the cytoplasm, where they are converted into siRNA by Dicer. TRBP2 plays a crucial role in recruiting Dicer to Ago2, ensuring the correct loading of siRNA duplexes [15]. Finally,

the siRNA is incorporated into the RISC [16]. The loading of siRNA into RISC is a complex process involving the RISC Loading Complex (RLC), thermodynamic sensing by Dicer, and localization at the rough endoplasmic reticulum (rER), all of which are essential for effective gene silencing [17]. The loading process of shRNA into RISC is approximately ten times more efficient than that of siRNA [18]. This suggests that a lower dose of shRNA is needed to maintain therapeutic efficacy while reducing off-target effects [18]. One potential limitation of RNAi in clinical applications is the challenge of delivering it into cells. Furthermore, shRNA provides more enduring silencing, simplifying delivery and reducing costs [16].

Respiratory syncytial virus (RSV) is a common cause of lower respiratory tract infections, often resulting in severe lung disease in infants due to inflammation and obstruction of small airways [19, 20]. RSV also poses a significant threat to immunocompromised individuals and the elderly [21]. The fusion protein (F) of RSV, which is highly conserved among the viral membrane proteins, can initiate infection on its own [22]. The F protein facilitates viral entry into cells and the fusion of infected cells with adjacent cells to form syncytia [23]. Previous studies have indicated that F protein expression can induce caspase-dependent cell death, suggesting its role as a potent inducer of apoptosis in RSV-infected cells [19]. This underscores the significance of the F protein in airway obstruction and the pathogenesis of RSV infection [19, 24].

Recent advancements in RSV treatment and prevention have led to the FDA approval of several vaccines, which have also been approved in some countries and regions for the elderly. These include Arexvy, ABRYSVO, and mRESVIA by GlaxoSmithKline (GSK), Pfizer, and Moderna, respectively. The CDC recommends these vaccines for adults aged 60 and older [25]. Additionally, monoclonal antibodies like Palivizumab and the long-acting RSV antibody Nirsevimab have been approved for prophylaxis in infants and children under 24 months [26, 27]. Several small-molecule antivirals targeting the fusion and polymerase proteins of RSV are in various stages of clinical development, though none have received approval yet [28]. Apart from ribavirin, a drug licensed by the WHO for RSV infection and primarily prescribed for hospitalized children, albeit with modest efficacy [29], effective antiviral drugs remain limited. This highlights the ongoing need for more effective treatments and underscores a critical gap in therapeutic options. In addition, there is a trend toward improved outcomes in patients receiving a combination of aerosolized ribavirin and an immunomodulator, rather than aerosolized ribavirin alone, as noted in prior studies [30–32]. Therefore, investigating the combination of ribavirin with gene-silencing technologies for treating RSV may present a strategy to enhance antiviral efficacy while potentially minimizing adverse effects by reducing the required dosage of ribavirin. While siRNA delivery using modified trans-acting activator of transcription (TAT) protein from human immunodeficiency virus 1 (HIV-1) is widespread [33–35], there have been no reports on the delivery of therapeutic shRNA against viral infections, including RSV, via penetratin peptide complexation. In this study, we developed a DNA vector expressing shRNA targeting the RSV F gene, which was delivered into virus-infected cells by penetratin. We evaluated its in vitro antiviral effects, including the inhibition of RSV replication and induction of cell apoptosis, and compared them to the effects of ribavirin.

Methods

Design and construction of RSV-F gene shRNA

The Biosettia online shRNA Designer tool (https://biosettia.com/shrna/) was used to design shRNA targeting the RSV-F gene to enhance shRNA functionality, reduce off-target effects, and stabilize the shRNA molecules. The designed shRNA was assessed using the BLAST tool at the NCBI database (http://blast.ncbi.nlm.nih.gov/) to compare the query sequence with the human genomic and transcript databases. The designed shRNA containing BamHI and HindIII restriction enzyme sites (GCAGTGCAGTCAGCAAAGGCTATCTTAGT-TCAA GAGGC-ACTAAGATAGCCTTTGCTGACTGCACTG C) was synthesized.

For expression in mammalian cells, the synthetic shRNA sequence was inserted into the pGFP-V-RS expression vector (CAT#: TR30007, OriGene Technologies, USA) after digestion with BamHI and HindIII, and ligated using T4 DNA ligase (Thermo Fisher Scientific, Waltham, MA, USA). This vector contains a U6 promoter for driving shRNA expression and a CMV promoter for driving the expression of green fluorescent protein (GFP), which serves as a marker for evaluating successful transfection and GFP expression. The resulting expression vector contained both the shRNA targeting the RSV-F gene and the GFP marker.

To amplify the expression vector, it was transformed into the *E. coli* strain DH5-α for further propagation. After colony PCR assays and enzyme digestion of selected single colonies, the plasmid containing the sequence of interest was subjected to Sanger sequencing for verification. The validated recombinant plasmids were amplified in *E. coli* DH5-α cells and purified using the GF1 nucleic acid extraction kit (Vivantis Technologies Co. Malaysia) according to the manufacturer's instructions. A non-effective 29-mer scrambled shRNA cassette in pGFP-V-RS vector (CAT#: TR30013, OriGene Technologies, USA) served as a negative control.

Preparation of penetratin/pGFP-V-RS containing shRNA complexes

Penetratin (RQIKIWFQNRRMKWKK) was synthesized by Proteogenix (France) with over 95% purity. The shRNA and penetratin peptide were prepared in stock solutions using HEPES-buffered saline (15 mmol/l HEPES, 150 mmol/l NaCl, pH 7.4). to create stock solutions. To prepare the complexes, the peptide solution was mixed with the pGFP-V-RS containing shRNA solution at different molar ratios (penetratin-shRNA ranging from 1:1 to 25:1), agitated briefly, and incubated at room temperature for 45 min to 1 h.

Gel retardation assay

An electrophoretic mobility shift assay (gel retardation assay) was used to assess shRNA incorporation by CPP into the complexes. For each solution prepared at different molar ratios of CPP and shRNA, 20 µL was mixed with 4 µL of 6X DNA loading buffer (containing 10 mM Tris-HCl, pH 7.6, 0.03% bromophenol blue, 0.03% xylene cyanol FF, 60% glycerol, and 60 mM EDTA), and then separated on a 1% agarose gel containing GelRed stain (Biotium, Cambridge, U.K.) in 0.5 M TBE buffer for 1 h at 90 V. The gel was photographed under UV light using a Vilber Lourmat gel documentation system (Vilber Lourmat, Collégien, France).

Size and zeta potential measurement

Penetratin-shRNA complexes were prepared in a total volume of 100 µL, as described earlier, at molar ratios of 5:1, 10:1, and 20:1 in 10 mM HEPES buffer (pH 7.4). The size of the freshly prepared complexes was determined by dynamic light scattering (DLS), and zeta potentials were measured using the electrophoretic method using the Zetasizer 3000 HS (Malvern Instruments, UK). Results are expressed as the average of three measurements.

Cell culture and virus propagation

Human epidermoid carcinoma of the larynx (HEp-2, NCBI code C144) and human lung cancer (A549, NCBI code C137) cells, possessing properties similar to normal airway epithelial cells, were obtained from the Pasteur Institute of Iran (Tehran, Iran). HEp-2 cells were grown in high-glucose Dulbecco's Modified Eagle Medium (DMEM, Gibco), while A549 cells were cultured in Dulbecco's Modified Eagle Medium/Nutrient Mixture F-12 (DMEM/F-12, Gibco). Both were supplemented with 10% fetal bovine serum (FBS), 100 units/mL penicillin, and 100 µg/mL streptomycin (Gibco), and incubated at 37 °C in an atmosphere of 5% CO_2. The human respiratory syncytial virus strain A2 (RSV A2, ATCC, VR-1540) was propagated in monolayer cultures of HEp-2 cells at 37 °C with 5% CO_2 in DMEM with 2% FBS. At 2–3 days post-infection (dpi), when cytopathic effects (CPE) were apparent, the cells underwent 2–3 rounds of freeze-thaw cycles to release the virus, followed by centrifugation at 3000 g for 10 min to remove cell debris. The harvested RSV was stored at -80 °C.

Virus titration

The tissue culture infectious dose 50 ($TCID_{50}$) was used to quantify the RSV titer. In 96-well plates, $8\times10^{\wedge3}$ HEp-2 cells per well were seeded in culture medium and incubated for approximately 24 h at 37 °C with 5% CO_2. When the cell confluence reached 80–90%, the RSV suspension (50 µL/well) serially diluted with DMEM was added in quadruplicate and infected for 2 h at 37 °C. The infected cells were then cultured in DMEM supplemented with 2% FBS at 37 °C with 5% CO_2 for 4–5 days. Staining was performed using crystal violet. 50% cell damage was taken as the critical point, and $TCID_{50}$ was calculated according to the Reed-Muench formula [36, 37]. Each plate contained a control group with non-infected cells. A positive cytopathic effect (CPE) was defined as compromising more than 30% of the cell monolayer [38]. Three independent experiments were performed for virus titration, and the Poisson distribution was applied to estimate plaque forming units (PFU) from $TCID_{50}$. The mean number of PFU/mL was estimated by multiplying the $TCID_{50}$ titer (per mL) by 0.7 [39]. The viral titer of the prepared stock was determined as $TCID_{50}$/mL and converted to PFU, resulting in a titer of $1.11\times10^{\wedge7}$ PFU/mL. The fifth-generation RSV strain A2 was selected for the experimental study based on the $TCID_{50}$ results. RSV A2 was used at a multiplicity of infection (MOI) of 0.1 for in vitro propagation experiments in HEp-2 and A549 cell.

Cellular internalization of penetratin/shRNA complexes

The day before treatment and transfection, HEp-2 cells were seeded into 24-well culture plates in high-glucose DMEM and incubated at 37 °C with 5% CO_2. When the cells reached 60–70% confluency, 50 µL of either penetratin/F-shRNA or penetratin/scramble-shRNA complexes were added to the cells. In a separate group, Lipofectamine 3000 (Thermo Fisher Scientific, Waltham, MA, USA) was used to deliver F-shRNA and scramble-shRNA into the cells, following the manufacturer's instructions. At 24 and 48 h post-transfection, GFP fluorescence in the cells was observed using fluorescence microscopy. Cells were directly examined under an Olympus microscope with a 10x objective lens (Olympus, Japan), and fluorescent images were captured using the GFP filter cube. Transfection efficiency was determined by counting green (transfected) cells and colorless (non-transfected) ones. Four images were taken at each time point and evaluated individually, with 100 cells per image.

To quantify the cellular uptake of shRNA, flow cytometry analysis was performed at 24 and 72 h after post-transfection for the different groups. The cells were washed twice with PBS, trypsinized using 0.1% (v/v) trypsin/EDTA in PBS, and centrifuged at 350 g for 5 min. After discarding the supernatant, the cell pellet was resuspended in 500 µL PBS. Flow cytometry analysis was performed immediately using a FACSCalibur flow cytometer (BD Biosciences; San Jose, California, USA). A total of 10,000 cells were analyzed per experiment, and the data were processed using FlowJo software version 10.0 (FlowJo LLC; USA). A549 cells were also subjected to fluorescence microscopy and flow cytometry to quantify the uptake of penetratin/shRNA complex and penetratin/scrambled-shRNA complexes.

Evaluation of cytotoxicity

The cytotoxicity of penetratin/shRNA complexes and ribavirin was tested using the MTT [(3-(4,5-dimethylthiazol-2-yl)-2,5-diphenyl tetrazolium bromide)] assay. Ten thousand HEp-2 cells were seeded into 96-well plates and cultured at 37 °C in a 5% CO_2 atmosphere incubator. Once the cells reached 70% confluence, the penetratin/shRNA complex (20:1, 25:1, 20 µL/well) and the penetratin/scramble-shRNA complex (20:1, 25:1, 20 µL/well) were added and incubated for 24, 48, and 72 h. Ribavirin (1–90 µM [40]) was incubated separately for 72 h. Subsequently, the culture medium was removed, 20 µL of MTT solution (Sigma-Aldrich, USA) was added, and the cells were incubated for 3–4 h until the purple precipitate became visible. The formazan was dissolved in dimethyl sulfoxide (DMSO) and quantified using a microplate reader at 570 nm according to the manufacturer's protocol. All presented data are based on experiments performed in triplicate.

Determination of silencing activity

To investigate the effect of various conditions on viral load reduction, three conditions were used: penetratin-shRNA, ribavirin (35 µM, as described in a previous study [40]), and the combination of penetratin-shRNA complex (20:1) with ribavirin (35 µM). Ninety thousand HEp-2 cells (in 0.5 mL DMEM with 10% FBS) were seeded into a 24-well plate and incubated overnight. The cells were then maintained in DMEM supplemented with 2% FBS for 1 h before virus inoculation, after which the virus inoculum (MOI = 0.1) was added to the wells. Four hours after virus propagation, different compounds were added to the cells in the three groups. The infected cell culture supernatant was harvested at 24 and 48 h post-treatment to evaluate the effect of the compounds using plaque assays and Real-time reverse transcription-polymerase chain reaction (RT-PCR).

Plaque assay

The viral titer was estimated in the supernatant of penetratin-shRNA complex- and ribavirin-treated RSV-infected HEp-2 cells using a plaque assay. Cells were plated at a density of 1.0×10^5 cells per well in 24-well plates and incubated at 37 °C with 5% CO_2 until 90% confluent cell monolayers were formed. The cells were then infected with the collected supernatant from the previous step (200 µL/well) and incubated for 2 h at 37 °C with 5% CO_2 to allow absorption, in duplicate. After incubation, the inocula were removed, and the monolayers were overlaid with 0.3% agarose in 1× DMEM supplemented with 2% FBS and 1% penicillin-streptomycin. Plates were incubated for 5 days at 37 °C with 5% CO_2. After incubation, the cells were fixed with 500 µL of 10% formaldehyde for 30 min and stained with a 1% crystal violet solution. Plaques were counted, and the average number of plaques from triplicate experiments was multiplied by the reciprocal of the dilution factor and divided by the inoculum volume (in mL). The result was expressed as PFU per mL.

Viral load quantitation

Total RNA was extracted from penetratin/shRNA complex- and ribavirin-treated RSV-infected HEp-2 cell culture supernatants using the RiboEx™ kit (GeneAll, Korea) according to the manufacturer's protocol. Two hundred nanograms of total RNA were used for cDNA synthesis with the PrimeScript RT reagent kit (TaKaRa, Japan) according to the manufacturer's instructions, in a total reaction volume of 10 µL. Briefly, the reaction was performed with 200 ng of total RNA and 0.1 µM of the RSV F1 gene-specific primer (5′-TAACCAGCAARGTGTTAGA-3′) for measuring RSV genomic RNA at 42 °C for 15 min.

The RSV load in the infected cell culture supernatant harvested at 24 h post-treatment was determined by absolute TaqMan® quantitative PCR. The RSV primers were as follows: RSV F1 primer: 5′-TAACCAGCAARGTGTTAGA-3′; RSV F2 primer: 5′-GATCATTTGTTATAGGCATATC-3′; and TaqMan® probe: FAM-CTATAGTAAATCAACAGAGTTGTCG-BHQ. The assay was performed using a Rotor-Gene Q platform (Qiagen) with 200 ng of template cDNA, 12.5 µl of RealQ Plus 2x Master Mix for Probe (Amplicon Odense M, Denmark), 0.4 µM of each primer, and 0.2 µM of the probe in a final volume of 25 µl. The amplification profile was as follows: 95 °C for 15 min, followed by 40 cycles of denaturation at 95 °C for 15 s, annealing at 55 °C for 30 s, and extension at 72 °C for 30 s.

Standard curve

To generate a standard curve for quantitative analysis, a 246 base-pair target PCR product was amplified using

forward and reverse primers of the F gene, as described previously, via reverse transcription-PCR from the RSV strain A2 (ATCC, VR-1540) stock. The PCR product was then cloned into the pTZ57R/T vector using the InsTA-clone PCR Cloning Kit (Thermo Scientific, USA). The obtained clones were evaluated by PCR and confirmed through Sanger sequencing. Plasmids were subsequently transformed into *E. coli* DH5α competent cells and purified using the GF-1 Plasmid DNA Extraction Kit (Vivantis Technologies, Malaysia). Quantification of the plasmids was performed in triplicate using a NanoDrop™ spectrophotometer (NanoDrop™ 2000; Thermo Scientific). Based on the plasmid concentration and the size of each linearized plasmid, the absolute copy number of DNA in each sample was calculated. The standard curve for virus quantification was generated using F gene-containing plasmids with 10-fold serial dilutions ranging from 3.76×10^10 to 376 copies/reaction. All curves were calculated based on the Ct values of the diluted standards using Rotor-Gene Q Series Software (QIAGEN, Germany, version 2.0.2). The detection limit was determined by the final dilution where the fluorescent signal was amplified exponentially, with a PCR Ct value of ≤40 set as the cutoff.

DNA fragmentation assay

DNA fragmentation assay was performed to detect apoptosis, as DNA fragmentation is a hallmark of this process. During the late stage of apoptosis, nuclear DNA is cleaved into fragments of 180–200 base pairs (bp), resulting in a characteristic ladder pattern on an agarose gel. The fragmentation of DNA into the characteristic apoptotic ladder was assessed as previously described [41]. A549 cells were seeded in a 24-well plate with RPMI medium. Once the cells reached 50–60% confluence, they were infected with RSV (MOI=0.1) for 2 h. The cells were then treated with a penetratin-shRNA complex (1:20, 50 µL/well) and ribavirin for 48 h. Following treatment, the cells were collected in 1.5 mL microcentrifuge tubes, washed once with 1 mL of 0.02% EDTA in PBS (without Ca^{2+} and Mg^{2+}), and pelleted by centrifugation at 350 g for 5 min. After centrifugation, 0.5 mL of lysis buffer (10 mM Tris-HCl, pH 7.5, 1 mM sodium-EDTA, 0.25% NP40) was added along with 0.1 mL of RNase A solution (10 mg/mL). The mixture was incubated for 20 min at 37 °C. Next, 0.1 mL of proteinase K solution (10 mg/mL) was added, and the samples were incubated for an additional 20 min. The samples were then analyzed by electrophoresis on a 1.8% agarose gel in TE buffer (40 mM Tris-acetate, 1 mM EDTA, pH 8.0) for 3 h at 36 V. GelRed™-stained DNA was visualized and photographed under UV light.

Propidium iodide staining

During apoptosis, endogenous nucleases cleave DNA into oligonucleosomal fragments, leading to dense, crescent-shaped chromatin aggregates the formation of apoptotic bodies [42]. Propidium iodide (PI) staining was performed to distinguish apoptotic cells from normal cells. A549 cells were infected with RSV and treated with penetratin-shRNA complex, penetratin-scramble complex, or a combination of penetratin-shRNA with ribavirin for 48 h. Cells were then washed with PBS and permeabilized with 0.1% Triton X-100 in PBS for 5 min at room temperature. The cells were stained with 10 µg/mL PI (Sigma) for 5 min, and fluorescent images were captured using fluorescence microscopy.

Caspase 3/7 activation assay

A549 cells were infected with RSV, treated, and harvested in 12-well plates as previously described. The caspase-3/7 activity in cell lysates after treatment was evaluated using the Caspase-3/7 Glo luminescent kit (Promega, USA) according to the manufacturer's instructions. Briefly, cells were lysed in TBS containing 1% Triton X-100 and 1 mM DTT. The cell lysate was then incubated with an equal volume of reagent in a white 96-well plate for 5 min at room temperature. Luminescence was measured using a Tecan Infinite M200 plate reader. Data are presented as the mean ± SD from three independent experiments.

Statistical analysis

All statistical analyses were performed using GraphPad Prism software version 8.0 (GraphPad Software Inc., La Jolla, CA, USA). Comparisons between two groups were assessed using the Student's t-test, while one-way analysis of variance (ANOVA) was employed for comparisons involving more than two groups. Results are expressed as the mean ± SD, and statistical significance set at $p<0.05$.

Results

Characterization of penetratin-shRNA complexes

A gel shift assay, followed by DNA visualization using autoradiography, was employed to determine the optimal molar ratio of the shRNA-encoding plasmid and CPP mixture for forming the most stable complex. In gel electrophoresis, small nucleic acid fragments migrate toward the anode more rapidly than those that have formed complexes with proteins. The data indicated that the optimal molar ratio of CPP to shRNA was 20:1. At this ratio, the migration of the peptide-DNA complex was completely blocked, and no free shRNA was detected on the agarose gel, indicating that the shRNA-encoding plasmid was fully complexed with penetratin (Fig. 1A and B).

To further characterize the penetratin-shRNA complexes, their size and charge were assessed using dynamic light scattering and zeta potential, to better understand

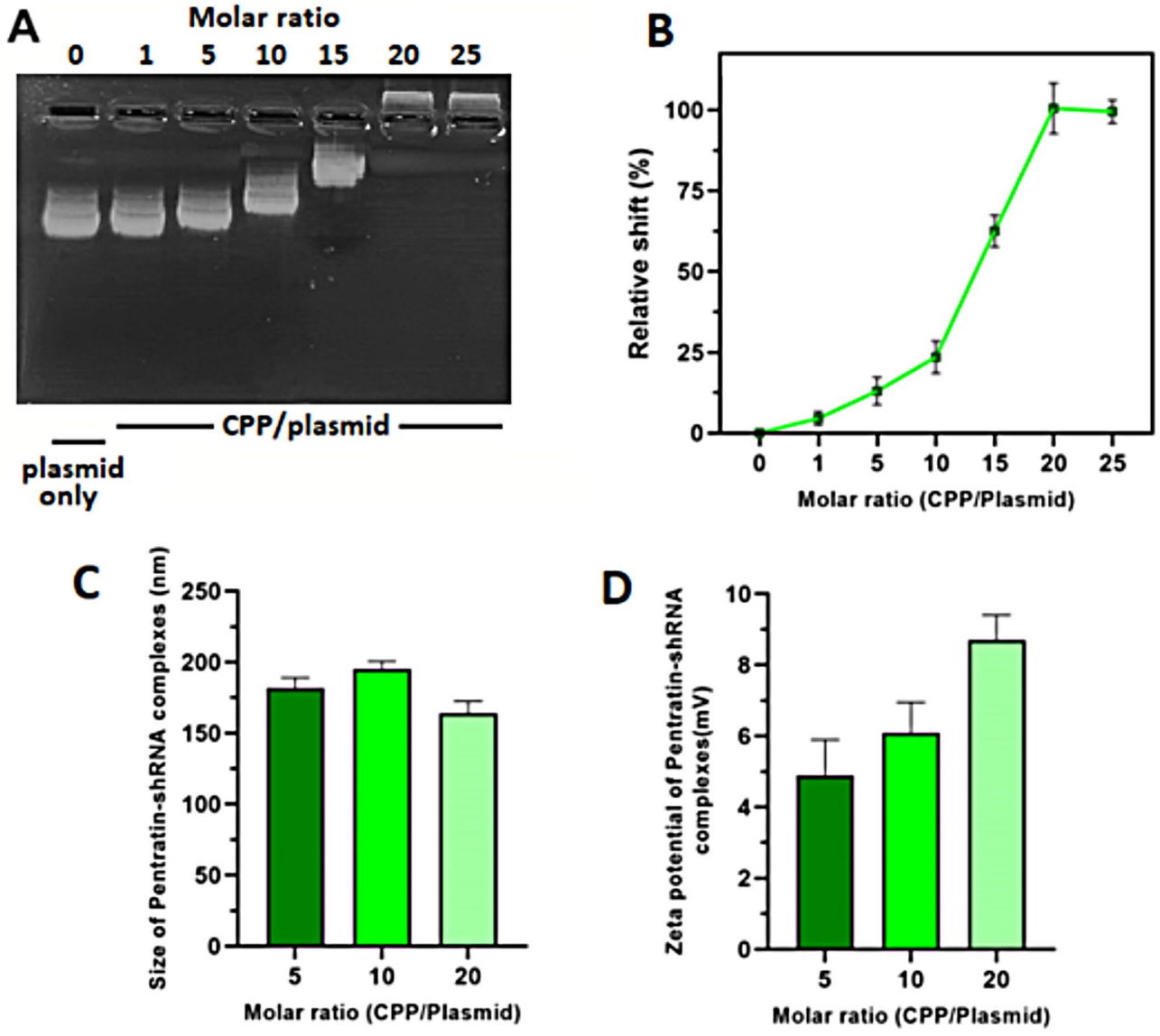

Fig. 1 Characterization of penetratin-shRNA complexes. (**A**) Gel retardation assay showing the formation of penetratin-shRNA complexes. Complexes of penetratin and shRNA-encoding plasmid were prepared at molar ratios of 1:1, 5:1, 10:1, 15:1, 20:1, and 25:1. These complexes were analyzed by agarose gel electrophoresis, followed by GelRed staining. (**B**) The relative mobility of penetratin-shRNA complexes is shown. Data are presented as mean ± SD from three independent experiments for each treatment group. The maximum shift was observed at a molar ratio of 20:1, which was used for subsequent analyses. (**C**) Size distribution spectrum of the penetratin-shRNA complex at a molar ratio of 20:1. (**D**) Zeta potential spectrum of the penetratin-shRNA complex at a molar ratio of 20:1

the physicochemical properties of the complexes. The size and charge were measured at CPP to shRNA molar ratios of 5:1, 10:1, and 20:1. The particle size of the penetratin-shRNA complex at a 20:1 ratio was 164 ± 16.5 nm (Fig. 1C), and the surface charge, or zeta potential, was 8.7 ± 1.2 mV (Fig. 1D). These findings were consistent with the gel retardation assay results for the CPP/DNA complexes.

Transfection efficiency of penetratin for shRNA delivery

Next, we investigated whether the complex could effectively deliver shRNA into cells. HEp-2 cells were incubated with the penetratin-shRNA complex, and transfection efficiency was assessed using a fluorescent dye and fluorescence microscopy. Transfected cells were imaged using fluorescent and transmitted light microscopy, and the transfection efficiency was calculated as the ratio of GFP-positive cells to the total number of cells. As shown in Fig. 2A, shRNA was successfully transfected into cells, with a strong green fluorescent signal observed. Transfection efficiency increased with the ratio of penetratin, reaching its peak at a 20:1 ratio (Table 1). Additionally, flow cytometry performed at 48 h post-transfection showed average transfection efficiencies

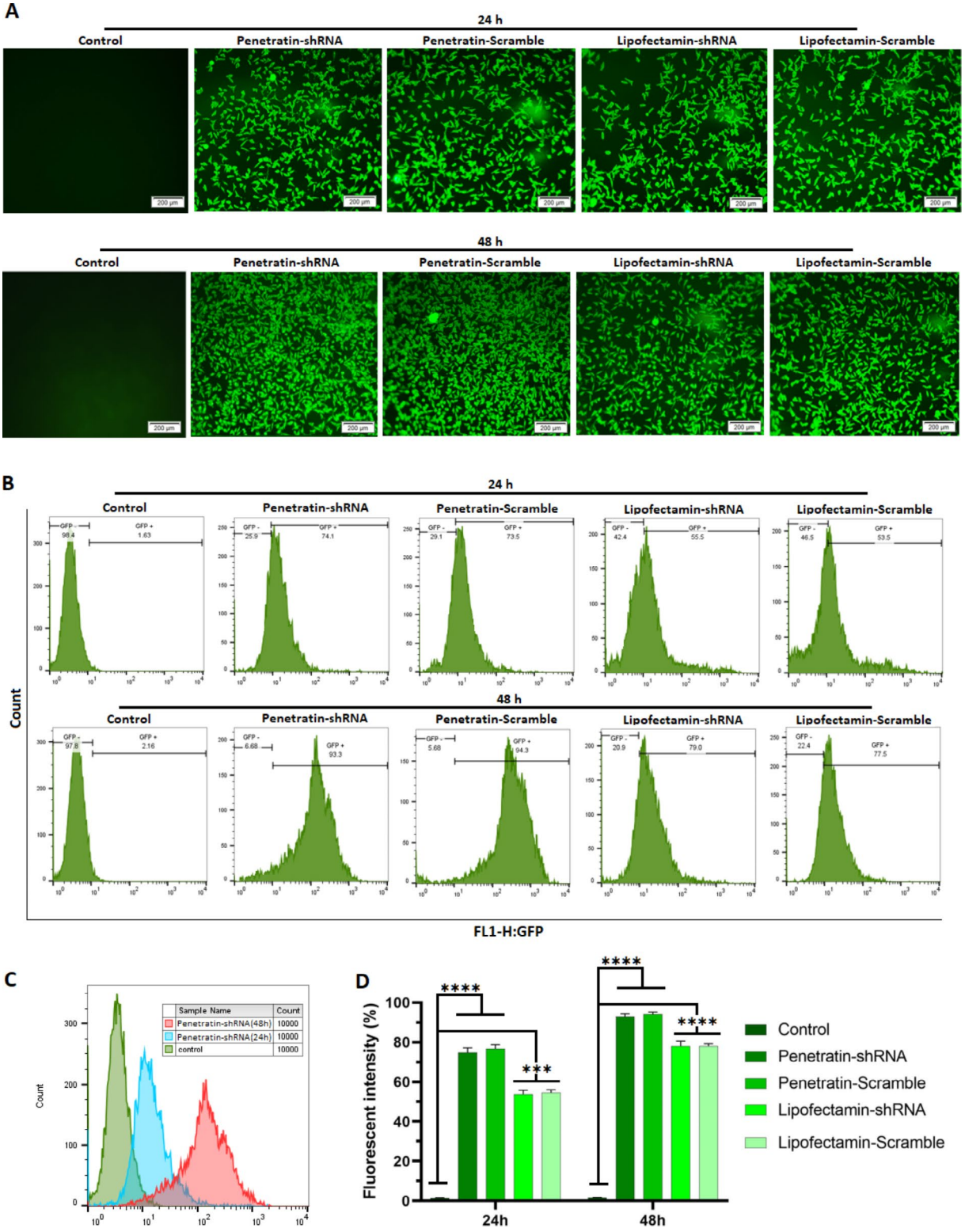

Fig. 2 Fluorescent intensity of penetratin-shRNA (20:1), penetratin-scramble (20:1), Lipofectamine-shRNA, and Lipofectamine-scramble, as analyzed by fluorescence microscopy and flow cytometry. (**A**) Fluorescence microscopy at 24 and 48 h post-transfection. Cells were observed using a 10x objective lens. (**B**) Histograms from FACS analysis for penetratin-shRNA, penetratin-scramble, Lipofectamine-shRNA, lipofectamine-scramble, and control groups after 24 and 48 h post-transfection. (**C**) Histograms from FACS analysis for penetratin-shRNA at 24 and 48 h post-transfection compared to the control group. (**D**) Average fluorescent intensity for different groups. Flow cytometry analysis revealed that the average fluorescent intensity for penetratin-shRNA transfected cells was 74.7% and 93% at 24 and 48 h, respectively

Table 1 The transfection efficiency of penetratin-shRNA at different molar ratios estimated by FACS 48 h post-transfection

Molar ratio of penetratin-shRNA	1:1	5:1	10:1	15:1	20:1	25:1	30:1
Transfection efficiency (%)	4.1 ± 0.8	15.2 ± 1.4	29.6 ± 3.1	73.5 ± 2.6	93 ± 1.7	93.6 ± 2.2	93.1 ± 1.9

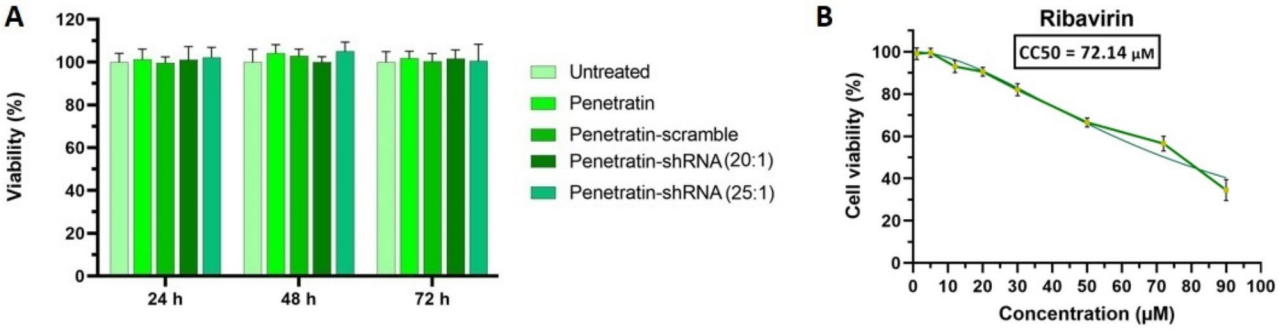

Fig. 3 Cell viability assay. (**A**) HEp-2 cells were exposed to penetratin-shRNA complexes and penetratin-scramble-shRNA at molar ratios of 20:1 and 25:1 for 24, 48, and 72 h. (**B**) Cytotoxicity assay of ribavirin at various concentrations in HEp-2 cells. Cells were treated with ribavirin at the indicated concentrations, and cytotoxicity was measured using the MTT assay after 3 days of incubation. Data represent the mean ± S.D. of three independent experiments

of 93% and 93.91% for penetratin-shRNA and penetratin-scramble complexes, respectively, as illustrated in Fig. 2B-D. Furthermore, when comparing the delivery efficiency of penetratin to that of Lipofectamine 3000, a significant difference was observed (74.7% vs. 53.8% at 24 h, $p<0.02$ and 93% vs. 78.1% at 48 h, $p<0.04$). These results confirm that penetratin is an effective vehicle for shRNA transfection into HEp-2 cells.

Cell viability is not affected by penetratin/shRNA complexes

An MTT assay was conducted to evaluate the cytotoxicity of penetratin-shRNA, penetratin-scramble, and ribavirin on HEp-2 cells. Cells were treated with the penetratin-shRNA complex (at 20:1 and 25:1 ratios), penetratin-scramble-shRNA (20:1 and 25:1), for 24, 48, and 72 h, and with ribavirin (1–90 µM) for 72 h. The MTT assay results are shown in Fig. 3. No significant cytotoxicity was observed in cells treated with penetratin-shRNA or penetratin-scramble complexes, even at the highest concentrations tested, when compared to untreated controls (Fig. 3A). In contrast, the 50% cytotoxic concentration (CC50) of ribavirin for HEp-2 cells was determined to be 72.14 µM, as measured by the MTT assay (Fig. 3B).

RSV infection in HEp-2 cells

Syncytia formation, a hallmark of RSV infection in HEp-2 cells [43], was examined. Clumps of unattached dead cells and multi-nucleated giant cells (syncytia) were observed in RSV-infected cells after 48 h post-infection. By the fifth day, syncytial cells were observed, and most cells were ruptured. The cells were harvested on the fifth dpi after showing 90% CPE (Fig. 4A). The morphology of the negative control cells remained unchanged, showing no signs of CPE. Additionally, the $TCID_{50}$ assay was performed to quantify the RSV titer in HEp-2 cells. This assay is considered representative for quantifying active, infectious viral particles. The RSV titer in HEp-2 cells was calculated to be 10^5.9 $TCID_{50}$/50 µL (Fig. 4B).

Penetratin-shRNA complex specifically silences the F gene of RSV in HEp-2 cells

Cells were treated with the penetratin-shRNA complex, ribavirin, and a combination of penetratin-shRNA with ribavirin, followed by RSV infection. Syncytia formation, an indicator of RSV infection was observed to assess the effectiveness of shRNA treatment. Untreated RSV-infected cells developed syncytia after 48 h, disrupting the HEp-2 cells monolayer. However, treatment with penetratin-shRNA complex significantly reduced syncytia formation, similar to ribavirin, but without the cytopathic effects typically associated with ribavirin. Uninfected HEp-2 cells treated with penetratin-shRNA showed no signs of cytotoxicity. Moreover, the combination of penetratin-shRNA and ribavirin further reduced syncytia formation compared to either treatment alone, while causing fewer cytopathic effects than ribavirin alone (Fig. 5A).

A CPE-based assay was used to evaluate ribavirin in dose-response experiments to determine the effective concentration (EC50). As shown in Fig. 5B, the EC50 value was 38.17 µM. Penetratin-shRNA showed no toxicity to HEp-2 cells, whereas ribavirin caused morphological changes and decreased monolayer density, with a CC50 of 72.14 µM (Fig. 3B). The CC50 values were at least 2 log10 higher than the EC50, indicating a favorable selectivity index (SI). Ribavirin had an SI (CC50/EC50) of 1.89.

The inhibitory effect of penetratin-shRNA on F gene expression was confirmed by real-time PCR, which

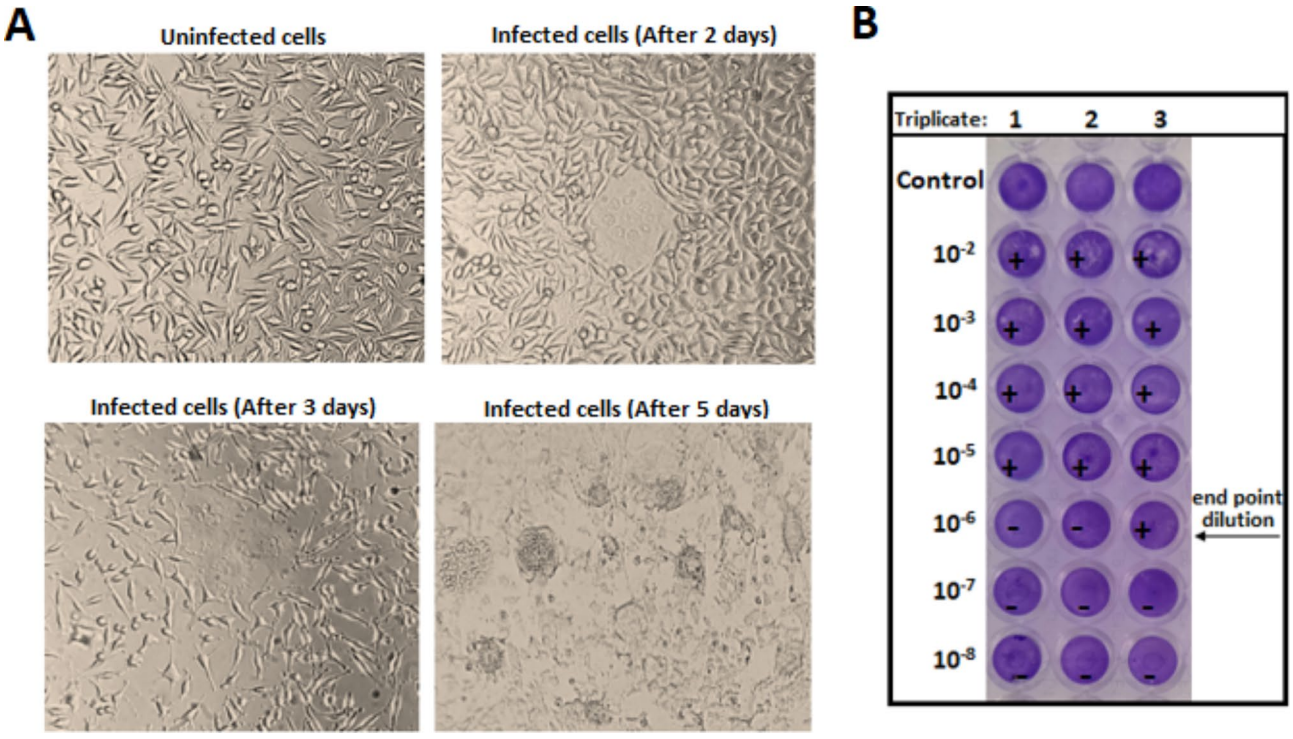

Fig. 4 RSV infection and TCID50. (**A**) HEp-2 cells showing syncytium formation at 2, 3, and 5 days post-infection with RSV. (**B**) The titer from the RSV sample was determined by TCID50. The 10^-6 dilution was the last one showing positive CPE for the RSV sample. "+" indicates positive CPE while "–" indicates no observed CPE

showed a reduction in F gene copy number from 8.8×10^5 in untreated cells to 5.45×10^3, 6.28×10^3, and 4.5×10^2 in cells treated with penetratin-shRNA, ribavirin, and both, respectively (Fig. 5C). These results demonstrate a significant reduction in RSV F gene copy numbers with penetratin-shRNA treatment compared to non-transfected cells ($p<0.0005$), indicating sequence-specific inhibition of RSV F gene expression in HEp-2 cells.

Penetratin-shRNA complex mediated inhibition of RSV production in HEp-2 cells

To assess the effect of penetratin-shRNA on the production of progeny virus, a plaque assay was performed on HEp-2 cell monolayers following treatment with penetratin-shRNA. RSV titer was determined by counting PFU. The results showed a titer of 1.8×10^6 PFU/mL in HEp-2 cell monolayers without treatment when infected with RSV. In contrast, lower viral titers were observed in wells treated with penetratin-shRNA after RSV infection. The viral titers ranged from 9.3×10^4 PFU/mL with ribavirin to 8.3×10^4 PFU/mL with penetratin-shRNA (Fig. 5D and E). When ribavirin was combined with penetratin-shRNA, the number of plaques further decreased to 4.35×10^3 PFU/mL. Viral titer values in wells treated with penetratin-shRNA were significantly reduced compared to non-transfected cells ($p<0.0005$).

Penetratin-shRNA complex mitigates DNA fragmentation in RSV infection

We first evaluated the transfection efficiency of penetratin-shRNA in A549 cells. As shown in Fig. 6A, successful shRNA transfection into A549 cells resulted in an intense green fluorescent signal, captured using fluorescence microscopy.

Next, we examined chromosomal DNA fragmentation, including smearing and laddering, in uninfected cells, RSV-infected cells, and RSV-infected cells treated with ribavirin or the penetratin-shRNA complex, using agarose gel electrophoresis. As depicted in Fig. 6B, DNA fragmentation was observed in infected cells, whereas nuclear DNA remained intact in uninfected cells and cells treated with the penetratin-shRNA complex. Notably, the degree of DNA fragmentation was reduced in RSV-infected cells treated with penetratin-shRNA compared to those treated with ribavirin or left untreated.

shRNA-penetratin Complex reduces the apoptosis in RSV-Infected A549 cells

To determine whether the shRNA-penetratin complex reduced apoptosis in infected A549 cells, we used the DNA-binding dye PI to observe apoptotic morphology. Apoptotic cells were identified by typical morphological changes such as cell shrinkage, chromatin condensation, membrane blebbing, DNA fragmentation, and the

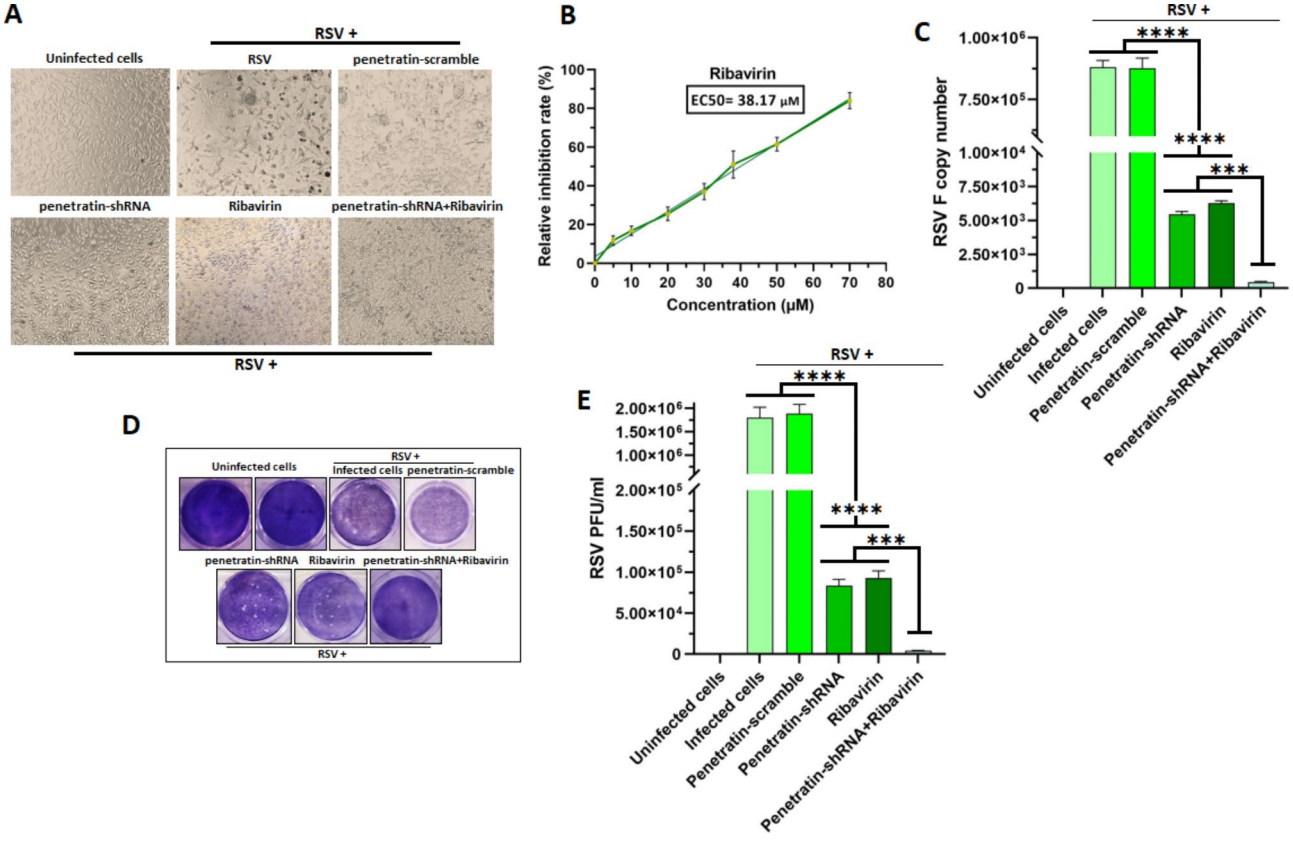

Fig. 5 Anti-viral activity of penetratin-shRNA, ribavirin, and their combination. (**A**) Protection of HEp-2 cells against RSV infection, visualized under a microscope. HEp-2 cells were infected with RSV (MOI = 0.1) and treated with penetratin-shRNA (20:1), penetratin-scramble (20:1), ribavirin (35 µM), or a combination of penetratin-shRNA and ribavirin. RSV infection CPE was observed using a 10x objective lens. (**B**) Relative inhibition rate of ribavirin in HEp-2 cells against RSV. (**C**) Real-time analysis of the F gene in different treatments of HEp-2 cells infected with RSV. Viral RNA was extracted 24 h post-transfection, and the F gene was quantified. Samples were analyzed in triplicate, and RSV F gene copy number is expressed as mean ± SD. (**D**) Plaque formation by RSV in HEp-2 cells in the presence of 0.3% agarose. HEp-2 cells were stained 5 days post-infection, following the established plaque-forming assay. (E) Plaque-forming units (PFU/ml) were counted 5 days after incubation. Experiments were repeated three times, and the virus titer is expressed as mean ± SD

formation of apoptotic bodies. PI staining revealed typical apoptotic features in RSV-infected A549 cells, with brightly red, condensed nuclei and apoptotic bodies, compared to uninfected cells, which displayed round, intact nuclei (Fig. 6C). Fluorescence images of infected cells treated with the shRNA-penetratin complex, or the combination of the shRNA-penetratin complex with ribavirin, showed a reduction in apoptotic morphology compared to untreated infected cells (Fig. 6C and D, $p<0.0001$). These results confirm characteristic nuclear fragmentation in the late stages of apoptosis.

As shown in Fig. 6E, caspase activity analysis revealed a significant increase in caspase 3/7 levels at 48 hpi in both untreated and penetratin-scramble-treated infected A549 cells, compared to uninfected cells. However, caspase 3/7 activity was significantly reduced in cells treated with the shRNA-penetratin complex compared to untreated RSV-infected cells ($p<0.0001$). Additionally, the combination of shRNA-penetratin complex and ribavirin significantly reduced apoptosis ($p<0.0001$). These findings are consistent with the results of inhibition experiments, as confirmed by DNA fragmentation and PI staining.

Discussion

Current therapeutic approaches for pulmonary RSV infection primarily focus on symptom management rather than disease eradicating. Ribavirin, an FDA-approved nucleoside analogue with anti-RSV properties, is a widely used therapeutic agent in most treatment guidelines globally. However, its effectiveness against the virus is debatable and limited, leading to its minimal use in clinical practice. Nonetheless, it serves as a benchmark for evaluating the efficacy of novel therapeutic interventions [44]. Therefore, there is an urgent need for new therapeutic approaches, including RNA interference (RNAi) strategies, which have shown significant promise [45]. siRNA has been studied for its impact on RSV replication due to its transient per-dose efficacy [46]. In contrast, shRNA offers sustained and highly efficient effects with fewer off-target effect outcomes, making it a preferred option for inhibiting RSV replication [18].

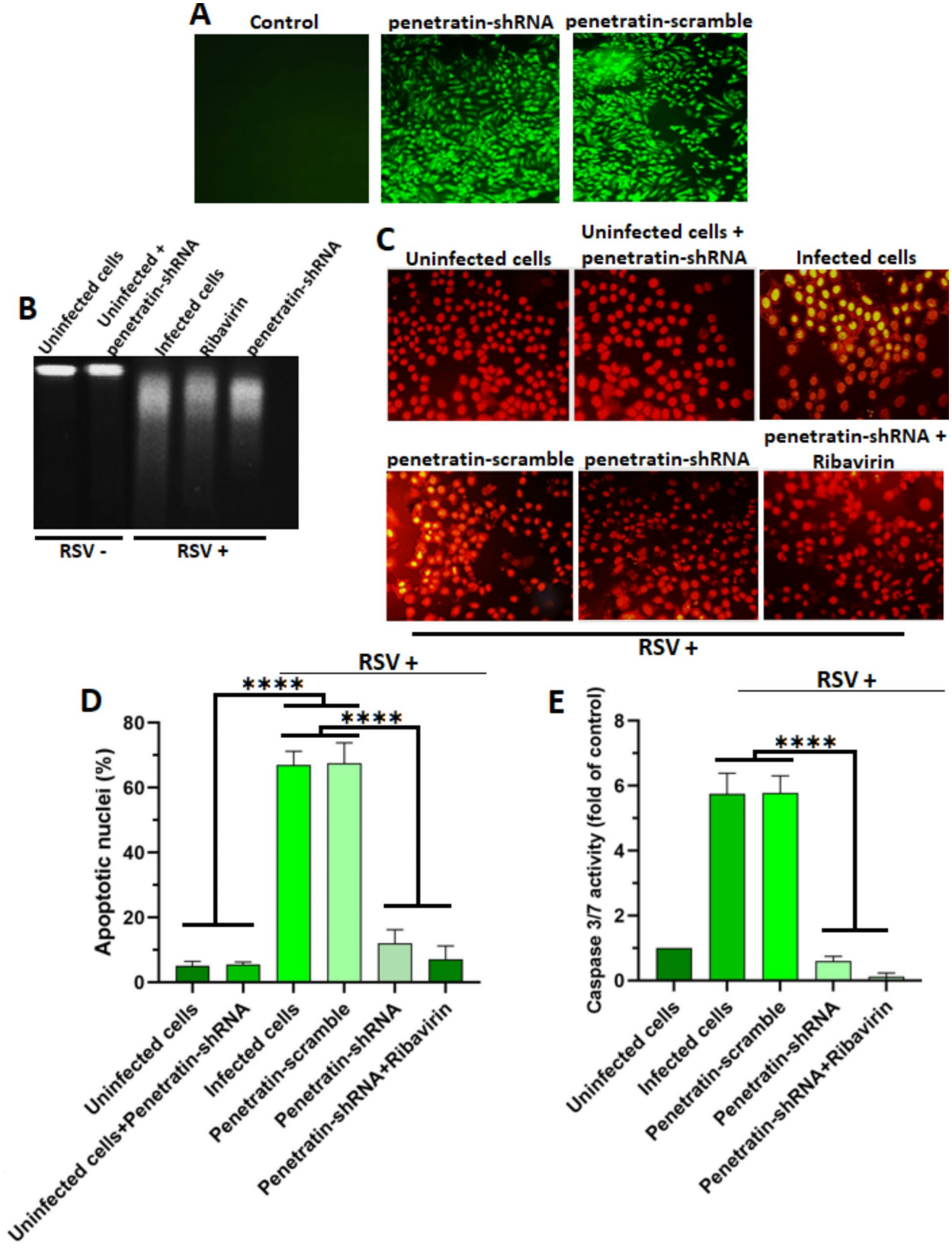

Fig. 6 (See legend on next page.)

(See figure on previous page.)

Fig. 6 (**A**) Fluorescence microscopy at 48 h post-transfection in A549 cells using a 10x objective lens. (**B**) DNA fragmentation in RSV-infected (MOI = 0.1) A549 cells. The hallmark of apoptosis, DNA fragmentation, was observed via GelRed staining. (**C**) Topological changes in nuclear particles in A549 cells. PI staining revealed the nuclear morphology in different groups of A549 cells under fluorescence microscopy. (**D**) Nuclear fragmentation and the presence of apoptotic bodies in A549 cells were observed as indicators of apoptosis. PI staining of uninfected A549 cells revealed normal nuclei with minimal debris, while infected-treated cells with penetratin-shRNA (20:1) and a combination of penetratin-shRNA with ribavirin showed decreased apoptotic signs compared to infected-untreated cells. (**E**) Caspase-3/7 activity in A549 cells. Caspase-3/7 activity in infected and non-infected A549 cells with various treatments was evaluated. The Caspase-3/7 activity in uninfected control groups was set to 1. At least two independent experiments were performed, and ratios are presented as mean ± SD

However, shRNA delivery into cells poses challenges compared to siRNA, primarily due to limitations in delivery methods. Viral vectors, commonly used in laboratories, face clinical limitations due to concerns about immunogenicity and safety [47, 48]. Using CPPs as non-viral vectors is a promising approach for effectively and non-invasively delivering shRNA into cells [49].

The potential of CPPs for molecular therapy is promising, particularly for delivering therapeutic agents such as nucleic acids, proteins, and small molecules in diseases like cancer and neurodegenerative disorders in vivo [50]. However, challenges remain in their clinical translation, including peptide stability, tissue-specific targeting, potential toxicity, and efficient endosomal escape [51]. Advances in CPP conjugation with nanoparticles and targeting ligands are improving delivery efficiency and reducing off-target effects [51]. Several CPP-based therapies have progressed through clinical trials, demonstrating efficacy and low toxicity [50]. For example, CPP-based therapies like p28 for cancer are currently in clinical trials, and ongoing research focuses on optimizing these systems for personalized medicine and gene therapy applications, including CRISPR-Cas9 delivery [51]. Recent studies highlight significant advancements, especially in gene therapy and cancer treatment. However, challenges persist, such as optimizing the balance between cell-specific penetration and minimizing off-target effects, largely due to the high positive charge of many CPPs [52]. Current research is focused on designing CPPs with tailored properties to improve biocompatibility and therapeutic outcomes [52, 53]. The integration of computational modeling is also expected to enhance understanding of CPP mechanisms, paving the way for more effective drug delivery systems [52].

In this study, we used penetratin as a cargo to introduce shRNA into cells, successfully delivering the vector into HEp-2 cells even at the highest concentration without causing specific toxicity. This finding is consistent with other cytotoxicity experiments, that reported an accurate IC50 for penetratin could not be obtained, even at concentrations up to 30 mM. Cell viability remained around 100% [54], indicating that penetratin did not inhibit cellular activity. Flow cytometry results demonstrated that using penetratin as a cargo for delivering plasmids containing shRNA was more effective under in vitro conditions compared to Lipofectamine (94.6% vs. 81.2%, respectively). Studies have shown that CPPs offer several advantages over Lipofectamine for plasmid delivery in vitro, and they have gained significant attention in drug delivery research due to their ability to efficiently penetrate cellular membranes with low cytotoxicity [55, 56]. Unlike Lipofectamine, which can negatively impact the catalytic activity of nucleic acids such as 10–23 DNAzyme, CPPs have been shown to maintain the catalytic performance of nucleic acids, making them a promising option for plasmid delivery [57]. Our previous study revealed that the complexation of therapeutic shRNA with the TAT peptide greatly improved intracellular plasmid delivery efficacy [58]. However, the current study demonstrates the superiority of penetratin over TAT for shRNA delivery due to its exceptional cellular uptake, leading to enhanced gene silencing efficiency. This might be explained by recent studies on the mechanism of penetratin uptake by cells, which indicate an almost exclusive endocytic uptake and vesicular localization of this peptide [59, 60]. Therefore, this study demonstrates that penetratin can be complexed with therapeutic shRNA to enhance cell transfection, providing an effective delivery platform for gene therapy with high efficiency and low cytotoxicity in cells.

Previous studies have demonstrated the potential of RNAi as an effective therapeutic approach for treating RSV infection [43]. Given its crucial role in viral entry and fusion [61], research on silencing the F gene of the virus has shown significant reduction in viral load, highlighting the RSV F-protein as a promising antiviral target [62–65]. In this study, we used specific shRNA molecules targeting a highly conserved region of the RSV F gene. Quantification of the F gene by real-time PCR revealed that shRNA can lead to substantial reduction in the RSV F gene in shRNA-transfected cells. The results showed that this construct reduced viral load by approximately 99.38%, compared to ribavirin, which reduced viral load by 99.28%. The combination of penetratin-shRNA and ribavirin treatments resulted in a 99.95% decrease in viral load, indicating that using penetratin-shRNA and ribavirin together has a significantly greater effect on reducing viral load than either treatment alone.

Additionally, to test whether the shRNA inhibited RSV production, we examined its effect on HEp-2 cells. Viral titers were estimated in shRNA transfected cells by performing a plaque assay on HEp-2 cells. The results show

that this treatment lowered viral titers by about 95.39%, slightly more than the 94.83% reduction achieved with ribavirin. The combined use of penetratin-shRNA and ribavirin resulted in a viral titer decrease of 99.76%. These findings suggest that specific penetratin-shRNA inhibits RSV viral progeny production in cultured HEp-2 cells. These results indicate that in the presence of penetratin-shRNA, newly transcribed F mRNA is degraded, leading to the inhibition of F protein synthesis. The absence of newly synthesized F protein hinders further virion production.

Apoptosis plays a dual role in virus-host interactions, being essential for eliminating abnormal cells and maintaining homeostasis [66]. However, viruses have evolved various strategies to hijack this cell death pathway, thereby promoting their own replication, assembly, and spread [67]. Research on RSV infection in A549 cells has revealed an increase in both pro- and anti-apoptotic factors, such as tumor necrosis factor-related apoptosis-inducing ligand (TRAIL) and its receptors, which sensitize infected cells to apoptosis through the TRAIL pathway [24]. At least three RSV proteins influence apoptotic mechanisms. The non-structural proteins 1 and 2 (NS1 and NS2) inhibit apoptosis in Vero cells through an IFN- and EGFR-independent pathway [68]. In contrast, the F protein of RSV plays a significant role in triggering p53-dependent apoptosis in epithelial cells, resulting in caspase-dependent cell death and subsequent loss of epithelial integrity [19]. Given its role as a prominent candidate for inducing apoptosis, the study also investigated the effect of silencing this gene using a penetratin-shRNA complex on the rate of apoptosis in A549 cells. The DNA fragmentation assay showed that untreated RSV-infected cells had the highest nuclear DNA fragmentation, indicating significant apoptosis. Treatment with the shRNA-penetratin complex reduced apoptosis compared to both untreated RSV-infected cells and those treated with ribavirin. PI staining confirmed decreased apoptotic morphology in RSV-infected cells treated with the shRNA-penetratin complex. Additionally, the complex significantly reduced caspase 3/7 activity. Overall, these findings suggest that the shRNA-penetratin complex inhibits apoptosis and limits virus release and spread in RSV-infected A549 cells. During its natural life cycle, RSV employs multiple strategies, such as lowering transcription factor p53 levels to prolong cell survival [69] and polarizing the distribution of the RSV F protein in epithelial cells [70], to delay early apoptosis for efficient virus replication. In contrast, the fusion activity of the F protein contributes to RSV pathogenesis by inducing apoptosis and shedding epithelial cells [19]. In line with previous studies, we found that RSV might exploit apoptosis during the late stage of its replication cycle. Therefore, inhibiting F protein production using shRNA will efficiently inhibit virus replication and prevent cell damage caused by F-triggered apoptosis.

Efficient delivery of DNA-conjugated peptides, particularly to the respiratory system, is complicated by its unique architecture and physiological barriers such as mucosal layers, immune clearance, and limited cellular uptake. Strategies to overcome these obstacles include the use of muco-penetrating nanoparticles, which enhance the passage through mucus and allow DNA-peptide complexes to reach target cells [51]. Additionally, nanoparticle carriers conjugated with CPPs improve stability, protect DNA from enzymatic degradation, and enhance tissue specificity when combined with ligand-based targeting [71]. Modifications to CPPs, such as pH-sensitive or fusogenic peptides, can also enhance endosomal escape, ensuring the DNA reaches the cytoplasm for proper expression [51]. To reduce immune clearance and increase circulation time, PEGylation or stealth nanoparticles can be employed [50]. Peptide-based vectors designed to target specific cells further improve transfection efficiency. For localized delivery, aerosolized inhalation therapies offer a promising approach, directly targeting the respiratory system and bypassing systemic barriers [72]. These combined strategies hold significant promise for improving the therapeutic efficacy of DNA-conjugated peptide systems, particularly in gene therapy and respiratory diseases. While the stability of the penetratin-shRNA complex was not directly evaluated in this study, it is a crucial factor that could influence the therapeutic efficacy of the complex. Previous studies have demonstrated that CPPs, including penetratin, enhance the stability of cargo molecules such as shRNA by protecting them from enzymatic degradation in biological environments [73–75]. However, additional research is required to assess the in vivo stability of the penetratin-shRNA complex, particularly in the presence of serum nucleases. The clinical efficacy of ribavirin therapy in severely ill infants and children remains controversial, with effectiveness observed primarily under high-dose and multiple short-duration administrations. However, the combination of ribavirin with an shRNA-penetratin complex, as shown in this study, promises to be a new treatment approach for RSV infections, potentially allowing for significantly reduced dosages. Further in vivo and clinical experiments are essential to confirm the effectiveness of this combination therapy and assess its potential clinical benefits.

Conclusions

In conclusion, this study highlights the efficacy of penetratin in delivering shRNA targeting the RSV F gene. The results are promising, showing a reduction in viral load, inhibition of virion production, and prevention of apoptosis-related cell damage in host cells. Notably,

this shRNA delivery method achieves these outcomes without causing toxicity and demonstrates superior performance compared to Lipofectamine in vitro. These findings underscore its potential for future therapeutic interventions, particularly in combination with ribavirin, against RSV infection.

Abbreviations

CC50	50% Cytotoxic Concentration
CPP	Cell-Penetrating Peptide
DLS	Dynamic Light Scattering
dpi	Days Post-infection
EC50	50% Effective Concentration
F	Fusion Gene (RSV F gene)
GFP	Green Fluorescent Protein
MOI	The Multiplicity of Infection
MTT	3-(4,5-Dimethylthiazol-2-yl)-2,5-Diphenyltetrazolium Bromide
PFU	Plaque-Forming Units
PI	Propidium Iodide
RSV	Respiratory Syncytial Virus
shRNA	Short Hairpin RNA
SI	Selectivity Index
$TCID_{50}$	Tissue Culture Infectious Dose 50

Acknowledgements
The authors thank BioRender (https://app.biorender.com/) for creating the graphical plots of schematic figure.

Author contributions
F.F. Experimentation and Methodology. H.A. Methodology, data validation, and original draft preparation. M.H.M. Statistical analysis and data interpretation. A.M. Consultation, data analysis and revision of the draft. A.F. Conceptualization, supervision, review, and editing. All authors reviewed the manuscript.

Funding
This study was supported by a grant from Shiraz University of Medical Sciences, Shiraz, Iran, under the Agreement No. 27957.

Data availability
No datasets were generated or analysed during the current study.

Declarations

Ethics approval and consent to participate
The research project has been approved by the Ethics Committee of Shiraz University of Medical Sciences (Approval ID: IR.SUMS.REC.1402.052).

Consent for publication
Not applicable.

Competing interests
The authors declare no competing interests.

Author details
[1]Division of Medical Biotechnology, Department of Medical Laboratory Sciences, School of Paramedical Sciences, Shiraz University of Medical Sciences, Shiraz, Iran
[2]Center for Cardiovascular Regeneration, Department of Cardiovascular Sciences, Houston Methodist Research Institute, Houston 77030, TX, USA
[3]Diagnostic Laboratory Sciences and Technology Research Center, School of Paramedical Sciences, Shiraz University of Medical Sciences, Shiraz, Iran

Received: 6 August 2024 / Accepted: 24 September 2024
Published online: 30 September 2024

References

1. Snyder EL, Dowdy SF. Cell penetrating peptides in drug delivery. Pharm Res. 2004;21:389–93. https://doi.org/10.1023/B:PHAM.0000019289.61978.f5.
2. Nasrollahi SA, Taghibiglou C, Azizi E, Farboud ES. Cell-penetrating peptides as a novel transdermal drug delivery system. Chem Biol Drug Des. 2012;80(5):639–46. https://doi.org/10.1111/cbdd.12008.
3. Saar K, Lindgren M, Hansen M, Eiríksdóttir E, Jiang Y, Rosenthal-Aizman K, Langel Ü. Cell-penetrating peptides: a comparative membrane toxicity study. Anal Biochem. 2005;345(1):55–65. https://doi.org/10.1016/j.ab.2005.07.033.
4. Lindgren M, Hällbrink M, Prochiantz A, Langel Ü. Cell-penetrating peptides. TIPS. 2000;21(3):99–103. https://doi.org/10.1016/s0165-6147(00)01447-4.
5. Margus H, Padari K, Pooga M. Cell-penetrating peptides as versatile vehicles for oligonucleotide delivery. Mol Ther. 2012;20(3):525–33. https://doi.org/10.1038/mt.2011.284. Epub 2012 Jan 10.
6. Deshayes S, Morris M, Heitz F, Divita G. Delivery of proteins and nucleic acids using a non-covalent peptide-based strategy. Adv Drug Deliv Rev. 2008;60(4–5):537–47. https://doi.org/10.1016/j.addr.2007.09.005.
7. Gros E, Deshayes S, Morris MC, Aldrian-Herrada G, Depollier J, Heitz F, Divita G. A non-covalent peptide-based strategy for protein and peptide nucleic acid transduction. Biochim Biophys Acta. 2006;1758(3):384–93. https://doi.org/10.1016/j.bbamem.2006.02.006.
8. Derossi D, Chassaing G, Prochiantz A. Trojan peptides: the penetratin system for intracellular delivery. Trends Cell Biol. 1998;8(2):84–7.
9. Fischer PM, Zhelev N, Wang S, Melville J, Fåhraeus R, Lane D. Structure–activity relationship of truncated and substituted analogues of the intracellular delivery vector Penetratin. J Pept Res. 2000;55(2):163–72. https://doi.org/10.1034/j.1399-3011.2000.00163.x.
10. Trabulo S, Cardoso AL, Mano M, De Lima MCP. Cell-penetrating peptides—mechanisms of cellular uptake and generation of delivery systems. Pharmaceuticals (Basel). 2010;3(4):961–93. https://doi.org/10.3390/ph3040961.
11. Lam JK, Chow MY, Zhang Y, Leung SW. siRNA versus miRNA as therapeutics for gene silencing. Mol Ther Nucleic Acids. 2015;4(9):e252. https://doi.org/10.1038/mtna.2015.23.
12. Liu YP, Berkhout B. miRNA cassettes in viral vectors: problems and solutions. Biochim Biophys Acta. 2011;1809(11–12):732–45. https://doi.org/10.1016/j.bbagrm.2011.05.014.
13. Sm E. Duplexes of 21-nucleotide RNAs mediate RNA interference in cultured mammalian cells. Nature. 2001;411(6836):494–8. https://doi.org/10.1038/35078107.
14. Aagaard L, Rossi JJ. RNAi therapeutics: principles, prospects and challenges. Adv Drug Deliv Rev. 2007;59(2–3):75–86. https://doi.org/10.1016/j.addr.2007.03.005.
15. Sakurai K, Amarzguioui M, Kim DH, Alluin J, Heale B, Song MS, Gatignol A, Behlke MA, Rossi JJ. A role for human dicer in pre-RISC loading of siRNAs. Nucleic Acids Res. 2011;39(4):1510–25. https://doi.org/10.1093/nar/gkq846.
16. Singh S, Narang AS, Mahato RI. Subcellular fate and off-target effects of siRNA, shRNA, and miRNA. Pharm Res. 2011;28(12):2996–3015. https://doi.org/10.1007/s11095-011-0608-1.
17. Stalder L, Heusermann W, Sokol L, Trojer D, Wirz J, Hean J, Fritzsche A, Aeschimann F, Pfanzagl V, Basselet P, Weiler J. The rough endoplasmatic reticulum is a central nucleation site of siRNA-mediated RNA silencing. EMBO J. 2013;32(8):1115–27. https://doi.org/10.1038/emboj.2013.52.
18. Rao DD, Vorhies JS, Senzer N, Nemunaitis J. siRNA vs. shRNA: similarities and differences. Adv Drug Deliv Rev. 2009;61(9):746–59. https://doi.org/10.1016/j.addr.2009.04.004.
19. Eckardt-Michel J, Lorek M, Baxmann D, Grunwald T, Keil GnM, Zimmer G. The fusion protein of respiratory syncytial virus triggers p53-dependent apoptosis. J Virol. 2008;82(7):3236–49. https://doi.org/10.1128/JVI.01887-07. Epub 2008 Jan 23.
20. Thompson WW, Shay DK, Weintraub E, Brammer L, Cox N, Anderson LJ, Fukuda K. Mortality associated with influenza and respiratory syncytial virus in the United States. JAMA. 2003;289(2):179–86. https://doi.org/10.1001/jama.289.2.179.
21. Falsey AR, Walsh EE. Respiratory syncytial virus infection in elderly adults. Drugs Aging. 2005;22(7):577–87. https://doi.org/10.2165/00002512-200522070-00004.
22. Tan L, Coenjaerts FE, Houspie L, Viveen MC, van Bleek GM, Wiertz EJ, Lemey P. The comparative genomics of human respiratory syncytial virus subgroups a and B: genetic variability and molecular evolutionary dynamics. J Virol. 2013;87(14):8213–26. https://doi.org/10.1128/JVI.03278-12.
23. Pastey MK, Crowe JE Jr, Graham BS. RhoA interacts with the fusion glycoprotein of respiratory syncytial virus and facilitates virus-induced

syncytium formation. J Virol. 1999;73(9):7262–70. https://doi.org/10.1128/JVI.73.9.7262-7270.1999.
24. Kotelkin A, Prikhod'ko EA, Cohen JI, Collins PL, Bukreyev A. Respiratory syncytial virus infection sensitizes cells to apoptosis mediated by tumor necrosis factor-related apoptosis-inducing ligand. J Virol. 2003;77(17):9156–72. https://doi.org/10.1128/jvi.77.17.9156-9172.2003.
25. Melgar M. Use of respiratory syncytial virus vaccines in older adults: recommendations of the Advisory Committee on Immunization Practices—United States, 2023. MMWR Morb Mortal Wkly Rep. 2023;72(29):793–801. https://doi.org/10.15585/mmwr.mm7229a4.
26. Jones JM, Fleming-Dutra KE, Prill MM, Roper LE, Brooks O, Sánchez PJ, Kotton CN, Mahon BE, Meyer S, Long SS, McMorrow ML. Use of Nirsevimab for the Prevention of Respiratory Syncytial Virus Disease among infants and Young children: recommendations of the Advisory Committee on Immunization Practices - United States, 2023. MMWR Morb Mortal Wkly Rep. 2023;72(34):920–5. https://doi.org/10.15585/mmwr.mm7234a4.
27. Hamid S, Winn A, Parikh R, Jones JM, McMorrow M, Prill MM, Silk BJ, Scobie HM, Hall AJ. Seasonality of respiratory Syncytial Virus - United States, 2017–2023. MMWR Morb Mortal Wkly Rep. 2023;72(14):355–61. https://doi.org/10.15585/mmwr.mm7214a1.
28. Felicetti T, Sarnari C, Gaito R, Tabarrini O, Manfroni G. Recent progress toward the Discovery of Small molecules as Novel Anti-respiratory Syncytial Virus agents. J Med Chem. 2024;67(14):11543–79. https://doi.org/10.1021/acs.jmedchem.4c00630.
29. Bonneux B, Jacoby E, Ceconi M, Stobbelaar K, Delputte P, Herschke F. Direct-acting antivirals for RSV treatment, a review. Antiviral Res. 2024;229:105948. https://doi.org/10.1016/j.antiviral.2024.105948.
30. Shah JN, Chemaly RF. Management of RSV infections in adult recipients of hematopoietic stem cell transplantation. Blood. 2011;117(10):2755–63. https://doi.org/10.1182/blood-2010-08-263400.
31. Ghosh S, Champlin RE, Englund J, Giralt SA, Rolston K, Raad I, Jacobson K, Neumann J, Ippoliti C, Mallik S, Whimbey E. Respiratory syncytial virus upper respiratory tract illnesses in adult blood and marrow transplant recipients: combination therapy with aerosolized Ribavirin and intravenous immunoglobulin. Bone Marrow Transpl. 2000;25(7):751–5. https://doi.org/10.1038/sj.bmt.1702228.
32. Mir WAY, Shrestha DB, Rana W, Yelma Reddy SR, Paudel A, Verda L. Successful treatment of respiratory syncytial virus infection in an immunocompromised patient with ribavirin. Cureus. 2021;13(8):e16930. https://doi.org/10.7759/cureus.16930.
33. Nakamura M, Fujiwara K, Doi N. Cytoplasmic delivery of siRNA using human-derived membrane penetration-enhancing peptide. J Nanobiotechnol. 2022;20(1):458. https://doi.org/10.1186/s12951-022-01667-4.
34. Danielson DC, Sachrajda N, Wang W, Filip R, Pezacki JP. A novel p19 Fusion protein as a delivery Agent for short-interfering RNAs. Mol Ther Nucleic Acids. 2016;5(4):e303. https://doi.org/10.1038/mtna.2016.14.
35. Li H, Zheng X, Koren V, Vashist YK, Tsui TY. Highly efficient delivery of siRNA to a heart transplant model by a novel cell penetrating peptide-dsRNA binding domain. Int J Pharm. 2014;469(1):206–13. https://doi.org/10.1016/j.ijpharm.2014.04.050.
36. Lei C, Yang J, Hu J, Sun X. On the calculation of TCID 50 for quantitation of virus infectivity. Virol Sin. 2021;36(1):141–4. https://doi.org/10.1007/s12250-020-00230-5. Epub 2020 May 26.
37. Lj R. A simple method of estimating fifty per cent endpoints. Am J Hyg. 1938;27:493–5.
38. Keiser PT, Anantpadma M, Staples H, Carrion R, Davey RA. Automation of infectious focus assay for determination of filovirus titers and direct comparison to plaque and TCID50 assays. Microorganisms. 2021;9(1):156. https://doi.org/10.3390/microorganisms9010156.
39. Stanley S, Hamel DJ, Wolf ID, Riedel S, Dutta S, Cheng A, Kanki PJ. Limit of detection for Rapid Antigen Testing of the SARS-CoV-2 Omicron variant. J Clin Microbiol. 2022;60(5):e0014022. https://doi.org/10.1128/jcm.00140-22.
40. Chung D-H, Moore BP, Matharu DS, Golden JE, Maddox C, Rasmussen L, Jia F. A cell based high-throughput screening approach for the discovery of new inhibitors of respiratory syncytial virus. Virol J. 2013;10:19. https://doi.org/10.1186/1743-422X-10-19.
41. Park DJ, Patek PQ. Detergent and enzyme treatment of apoptotic cells for the observation of DNA fragmentation. Biotechniques. 1998;24(4):558–60. https://doi.org/10.2144/98244bm07.
42. Nicoletti I, Mannucci R. Fluorescence Microscopy Analysis of Nuclear Alterations during Apoptosis, vol. 4 of Purdue Cytometry CD-ROM Series. Istituto di Medicina Interna e Scienze Oncologiche, Universita di Perugia, Perugia, Italy. 2002;4.
43. Bitko V, Barik S. Phenotypic silencing of cytoplasmic genes using sequence-specific double-stranded short interfering RNA and its application in the reverse genetics of wild type negative-strand RNA viruses. BMC Microbiol. 2001;1:34. https://doi.org/10.1186/1471-2180-1-34.
44. Kim YI, Pareek R, Murphy R, Harrison L, Farrell E, Cook R, DeVincenzo J. The antiviral effects of RSV fusion inhibitor, MDT-637, on clinical isolates, vs its achievable concentrations in the human respiratory tract and comparison to Ribavirin. Influenza Other Respir Viruses. 2017;11(6):525–30. https://doi.org/10.1111/irv.12503.
45. Kim D, Rossi J. RNAi mechanisms and applications. Biotechniques. 2008;44(5):613–6. https://doi.org/10.2144/000112792.
46. Xing Y, Proesmans M. New therapies for acute RSV infections: where are we? Eur J Pediatr. 2019;178(2):131–8. https://doi.org/10.1007/s00431-018-03310-7.
47. Lundstrom K. Are viral vectors any good for RNAi antiviral therapy? Viruses. 2020;12(10):1189. https://doi.org/10.3390/v12101189.
48. Robbins PD, Tahara H, Ghivizzani SC. Viral vectors for gene therapy. Trends Biotechnol. 1998;16(1):35–40. https://doi.org/10.1016/S0167-7799(97)01137-2.
49. Endoh T, Ohtsuki T. Cellular siRNA delivery using cell-penetrating peptides modified for endosomal escape. Adv Drug Deliv Rev. 2009;61(9):704–9. https://doi.org/10.1016/j.addr.2009.04.005.
50. Timotievich ED, Shilovskiy IP, Khaitov MR. Cell-penetrating peptides as vehicles for delivery of therapeutic nucleic acids. Mechanisms and application in Medicine. Biochem (Mosc). 2023;88(11):1800–17. https://doi.org/10.1134/S0006297923110111.
51. Zahid M, Robbins PD. Cell-type specific penetrating peptides: therapeutic promises and challenges. Molecules. 2015;20(7):13055–70. https://doi.org/10.3390/molecules200713055.
52. Ivánczi M, Balogh B, Kis L, Mándity I. Molecular Dynamics simulations of Drug-conjugated cell-penetrating peptides. Pharmaceuticals (Basel). 2023;16(9):1251. https://doi.org/10.3390/ph16091251.
53. Ghaemi B, Tanwar S, Singh A, Arifin DR, McMahon MT, Barman I, Bulte JWM. Cell-penetrating and enzyme-responsive peptides for targeted Cancer Therapy: role of arginine residue length on cell penetration and in vivo systemic toxicity. ACS Appl Mater Interfaces. 2024;16(9):11159–71. https://doi.org/10.1021/acsami.3c14908.
54. Liu C, Tai L, Zhang W, Wei G, Pan W, Lu W. Penetratin, a potentially powerful absorption enhancer for noninvasive intraocular drug delivery. Mol Pharm. 2014;11(4):1218–27. https://doi.org/10.1021/mp400681n.
55. Asrorov AM, Wang H, Zhang M, Wang Y, He Y, Sharipov M, Huang Y. Cell penetrating peptides: highlighting points in cancer therapy. Drug Dev Res. 2023;84(6):1037–71. https://doi.org/10.1002/ddr.22076.
56. Liu H, Li Y, Du S, Wang C, Li Y, Cao R, He J. Studies on the effect of Lipofectamine and cell-penetrating peptide on the properties of 10–23 DNAzyme. Molecules. 2023;28(9):3942. https://doi.org/10.3390/molecules28093942.
57. Rai A, Jerath G. Cell-penetrating peptides. De Novo Pept Des. 2023;105–31. https://doi.org/10.1016/B978-0-323-99917-5.00005-6.
58. Fard SAZ, Abuei H, Behbahani AB, Rafiei Dehbidi G, Zare F, Nejabat M, et al. Unlocking therapeutic potential: enhanced shRNA delivery with Tat peptide in the human respiratory Syncytial Virus Treatment. Adv Pharm Bull. 2024;14(3). https://doi.org/10.34172/apb.2024.045.
59. Duchardt F, Fotin-Mleczek M, Schwarz H, Fischer R, Brock R. A comprehensive model for the cellular uptake of cationic cell-penetrating peptides. Traffic. 2007;8(7):848–66. https://doi.org/10.1111/j.1600-0854.2007.00572.x.
60. Maiolo JR, Ferrer M, Ottinger EA. Effects of cargo molecules on the cellular uptake of arginine-rich cell-penetrating peptides. Biochim Biophys Acta. 2005;1712(2):161–72. https://doi.org/10.1016/j.bbamem.2005.04.010.
61. Leemans A, Boeren M, Van der Gucht W, Pintelon I, Roose K, Schepens B, Caljon G. Removal of the N-glycosylation sequon at position N116 located in p27 of the respiratory syncytial virus fusion protein elicits enhanced antibody responses after DNA immunization. Viruses. 2018;10(8):426. https://doi.org/10.3390/v10080426.
62. Malekshahi SS, Salimi V, Arefian E, Fatemi-Nasab G, Adjaminejad-Fard S, Yavarian J, Mokhtari-Azad T. Inhibition of respiratory syncytial virus replication by simultaneous targeting of mRNA and genomic RNA using dual-targeting siRNAs. Mol Biotechnol. 2016;58(11):767–75. https://doi.org/10.1007/s12033-016-9976-4.
63. Martín-Vicente M, Resino S, Martínez I. siRNA-mediated simultaneous regulation of the cellular innate immune response and human respiratory syncytial

virus replication. Biomolecules. 2019;9(5):165. https://doi.org/10.3390/biom9050165.
64. Vig K, Lewis N, Moore EG, Pillai S, Dennis VA, Singh SR. Secondary RNA structure and its role in RNA interference to silence the respiratory syncytial virus fusion protein gene. Mol Biotechnol. 2009;43(3):200–11. https://doi.org/10.1007/s12033-009-9190-8.
65. Zadeh SA, Abuei H, Farhadi A, Dehbidi GR, Zare F, Nejabat M, Behbahani AB. Sustained suppression of fusion gene-mediated human respiratory syncytial virus load by shRNA-based therapeutics. BBRJ. 2023;3464–70. https://doi.org/10.4103/bbrj.bbrj_163_23.
66. Neumann S, El Maadidi S, Faletti L, Haun F, Labib S, Schejtman A, Borner C. How do viruses control mitochondria-mediated apoptosis? Virus Res. 2015;209:45–55. https://doi.org/10.1016/j.virusres.2015.02.026.
67. Benedict CA, Norris PS, Ware CF. To kill or be killed: viral evasion of apoptosis. Nat Immunol. 2002;3(11):1013–8. https://doi.org/10.1038/ni1102-1013.
68. Bitko V, Shulyayeva O, Mazumder B, Musiyenko A, Ramaswamy M, Look DC, Barik S. Nonstructural proteins of respiratory syncytial virus suppress premature apoptosis by an NF-κB-dependent, interferon-independent mechanism and facilitate virus growth. J Virol. 2007;81(4):1786–95. https://doi.org/10.1128/JVI.01420-06.
69. Groskreutz DJ, Monick MM, Yarovinsky TO, Powers LS, Quelle DE, Varga SM, Look DC, Hunninghake GW. Respiratory syncytial virus decreases p53 protein to prolong survival of airway epithelial cells. J Immunol. 2007;179(5):2741–7. https://doi.org/10.4049/jimmunol.179.5.2741.
70. Brock SC, Goldenring JR, Crowe JE Jr. Apical recycling systems regulate directional budding of respiratory syncytial virus from polarized epithelial cells. Proc Natl Acad Sci U S A. 2003;100(25):15143–8. https://doi.org/10.1073/pnas.2434327100.
71. Wang X, Cai C, Lv W, Chen K, Li J, Liao K, Zhang Y, Huang H, Lin Y, Rong Z, Duan X. Short cell-penetration peptide conjugated bioreducible polymer enhances gene editing of CRISPR system. J Nanobiotechnol. 2024;22(1):284. https://doi.org/10.1186/s12951-024-02554-w.
72. Xiang K, Li Y, Cong H, Yu B, Shen Y. Peptide-based non-viral gene delivery: a comprehensive review of the advances and challenges. Int J Biol Macromol. 2024;266(Pt 1):131194. https://doi.org/10.1016/j.ijbiomac.2024.131194.
73. Silhol M, Tyagi M, Giacca M, Lebleu B, Vivès E. Different mechanisms for cellular internalization of the HIV-1 Tat-derived cell penetrating peptide and recombinant proteins fused to Tat. Eur J Biochem. 2002;269(2):494–501. https://doi.org/10.1046/j.0014-2956.2001.02671.x.
74. Rittner K, Benavente A, Bompard-Sorlet A, Heitz F, Divita G, Brasseur R, Jacobs E. New basic membrane-destabilizing peptides for plasmid-based gene delivery in vitro and in vivo. Mol Ther. 2002;5(2):104–14. https://doi.org/10.1006/mthe.2002.0523.
75. Simeoni F, Morris MC, Heitz F, Divita G. Insight into the mechanism of the peptide-based gene delivery system MPG: implications for delivery of siRNA into mammalian cells. Nucleic Acids Res. 2003;31(11):2717–24. https://doi.org/10.1093/nar/gkg385.

Publisher's note